Inorg. Chem. **2002**, *41*, 6973–6985

Electronic Spectra and Structures of d^2 Molybdenum–Oxo Complexes. Effects of Structural Distortions on Orbital Energies, Two-Electron Terms, and the Mixing of Singlet and Triplet States

Ryan E. Da Re and Michael D. Hopkins*

Department of Chemistry, University of Chicago, 5735 S. Ellis Avenue, Chicago, Illinois 60637

Received September 16, 2002

Molybdenum–oxo ions of the type $[Mo^{IV}OL_4Cl]^+$ (L = $CNBu^t$, PMe_3, $^1/_2Me_2PCH_2CH_2PMe_2$) have been studied by X-ray crystallography, vibrational spectroscopy, and polarized single-crystal electronic absorption spectroscopy (300 and ca. 20 K) in order to investigate the effects of the ancillary ligand geometry on the properties of the Mo≡O bond. The idealized point symmetries of the $[Mo^{IV}OL_4Cl]^+$ ions were established by X-ray crystallographic studies of the salts $[MoO(CNBu^t)_4Cl][BPh_4]$ (C_{4v}), $[MoO(dmpe)_2Cl]Cl\cdot 5H_2O$ (C_{2v}), and $[MoO(PMe_3)_4Cl][PF_6]$ (C_{2v}); the lower symmetries of the phosphine derivatives are the result of the steric properties of the phosphine ligands. The Mo≡O stretching frequencies of these ions (948–959 cm^{-1}) are essentially insensitive to the nature and geometry of the equatorial ligands. In contrast, the electronic absorption bands arising from the nominal $d_{xy} \rightarrow d_{xz}, d_{yz}$ (n → π^*(MoO)) ligand-field transition exhibit a large dependence on the geometry of the equatorial ligands. Specifically, the electronic spectrum of $[MoO(CNBu^t)_4Cl]^+$ exhibits a single $^1[n \rightarrow \pi^*_{xz,yz}]$ band, whereas the spectra of both $[MoO(dmpe)_2Cl]^+$ and $[MoO(PMe_3)_4Cl]^+$ reveal separate $^1[n \rightarrow \pi^*_{xz}]$ and $^1[n \rightarrow \pi^*_{yz}]$ bands. A general theoretical model of the n → π^* state energies of structurally distorted d^2 M(≡E)L_4X chromophores is developed in order to interpret the electronic spectra of the phosphine derivatives. Analysis of the n → π^* transition energies using this model indicates that the d_{xz} and d_{yz} π^*(Mo≡O) orbitals are nondegenerate for the C_{2v}-symmetry ions and the n → π^*_{xz} and n → π^*_{yz} excited states are characterized by different two-electron terms. These effects lead to a significant redistribution of intensity between certain spin-allowed and spin-forbidden absorption bands. The applicability of this model to the excited states produced by $\delta \rightarrow \pi$ and $\pi \rightarrow \delta$ symmetry electronic transitions of other chromophores is discussed.

Introduction

The great importance of metal−oxo complexes in catalysis, synthesis, and biochemistry has motivated numerous investigations of the nature of M−O multiple bonds over the past four decades.[1,2] Our understanding of these bonds is based largely on experimental and theoretical studies of the large class of d^1- and d^2-configured metal−oxo complexes that possess 4-fold axial symmetry. The electronic structures of these five- and six-coordinate complexes are typically described in terms of the d-orbital splitting pattern originally proposed by Jørgensen, Ballhausen, and Gray to explain the bonding in the molybdenyl and vanadyl ions.[3,4]

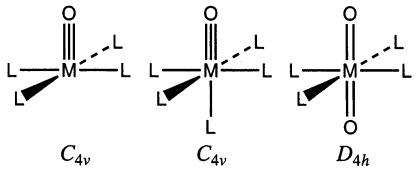

In this picture, the t_{2g}-parentage d orbitals of O_h-symmetry ML_6 are split under the strong axial compression of the oxo ligand(s): the degenerate d_{xz} and d_{yz} orbitals, which are principally M−O π-antibonding in nature, are destabilized relative to the d_{xy} orbital, which is nonbonding (δ symmetry) with respect to the M−O axis. Thus, monooxo complexes possess formal M≡O bonds, and dioxo complexes possess formal M═O bonds. Numerous experimental and theoretical studies have borne out this picture;[1,5−7] combined, the two original studies[3,4] have been cited in the literature 1400 times.

* To whom correspondence is addressed. E-mail: mhopkins@uchicago.edu.

(1) Nugent, W. A.; Mayer, J. M. *Metal−Ligand Multiple Bonds*; Wiley: New York, 1988.
(2) Hille, R. *Chem. Rev.* **1996**, *96*, 2757−2816.
(3) Jørgensen, C. K. *Acta Chem. Scand.* **1957**, *11*, 73−85.
(4) Ballhausen, C. J.; Gray, H. B. *Inorg. Chem.* **1962**, *1*, 111−122.

10.1021/ic020565r CCC: $22.00
Published on Web 12/05/2002

Few metal−oxo compounds (or complexes with other multiply bonded ligands) possess the high point symmetries of the model complexes for which this bonding picture was developed. Thus, it is important to understand the electronic structures of lower-symmetry complexes in order to compare the natures of metal−oxygen multiple bonds and other types of metal−ligand multiple bonds in real (as opposed to hypothetical) molecules. A key case in point is the class of d^2 multiply bonded complexes with ancillary phosphine ligands, of the general forms *trans*-$ME(PR_3)_4X$ and *trans*-$ME_2(PR_3)_4$ (M = Ta, Cr, Mo, W, Mn, Tc, Re; X = halide or pseudohalide; PR_3 = monodentate or $^1/_2$ bidentate phosphine), which have been the subject of numerous theoretical and electronic spectroscopic studies.[8−13] These complexes have attracted interest because they span an extremely broad range of multiply bonded ligands (E = O,[1] N,[1] NR,[14] CR,[15] CR_2,[16] S,[17] Se,[17] Te,[17] GeR[18]), thus allowing direct comparisons to be made among different multiple bonds under a constant ancillary ligand field. The electronic structures of *trans*-$MO(PR_3)_4X$ and *trans*-$MO_2(PR_3)_4$ complexes are the benchmarks for these studies, because of the much deeper general understanding of M−O bonds.

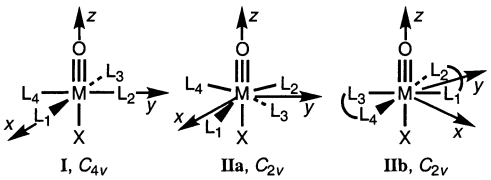

Figure 1. Structural types and molecular coordinate systems of MOL_4X complexes. For **I**, the coordinating L atoms lie in the *xz*- and *yz*-planes and below the *xy*-plane. For **IIa**, L_1 and L_3 lie in the *xz*-plane and below the *xy*-plane, and L_2 and L_4 lie in the *yz*-plane and above the *xy*-plane. For **IIb**, the L atoms are bisected by the *xz*- and *yz*-planes and lie below the *xy*-plane.

Prior studies of the electronic structures and spectra of *trans*-$ME(PR_3)_4X$ and *trans*-$ME_2(PR_3)_4$ complexes have typically invoked the approximation that their structures possess effective 4-fold axial symmetry (**I**, Figure 1), even though all structurally characterized examples of these complexes are significantly distorted from this limit. X-ray crystallographic studies have revealed these structural distortions to be of two main types. For derivatives with monodentate phosphines, such as PMe_3, the phosphorus nuclei adopt a pseudo S_4 arrangement about the metal center to relieve the steric repulsion among the phosphine ligands. This distortion, illustrated in Figure 1 for a $MO(PR_3)_4X$ complex (**IIa**), reduces the maximal symmetry to C_{2v}. For chelating phosphines ($R_2P{\sim}PR_2$), of which the prevalent examples are those with two carbon atoms in the backbone, the structural constraints imposed by the backbone allow the phosphorus nuclei to lie closer to coplanarity but result in different P−M−P angles within and between the ligands. This reduces the maximum symmetry of *trans*-$MO(R_2P{\sim}PR_2)_2X$ to C_{2v} (**IIb**, Figure 1). The general electronic consequence of these distortions for the M−E bonds is that their π-symmetry orbitals are no longer required to be degenerate. Claims in the literature that the splittings of these orbitals are, or should be, small have not been tested experimentally.

The purpose of the present study is to examine the effects of systematic structural distortions on the electronic structures and spectra of metal−oxo complexes. We report the crystal structures, vibrational spectra, and polarized single-crystal electronic absorption spectra of three prototypical d^2 ions of the type $[MoOL_4Cl]^+$: $[MoO(CNBu^t)_4Cl]^+$, which is an example of C_{4v}-symmetry structure type **I**, and the C_{2v}-symmetry phosphine derivatives $[MoO(PMe_3)_4Cl]^+$ (**IIa**) and $[MoO(dmpe)_2Cl]^+$ (**IIb**; dmpe = 1,2-bis(dimethylphosphi-

(5) Miskowski, V. M.; Gray, H. B.; Hopkins, M. D. *Adv. Transition Met. Coord. Chem.* **1996**, *1*, 159−186.
(6) (a) Savoie, C.; Reber, C. *J. Am. Chem. Soc.* **2000**, *122*, 844−852. (b) Savoie, C.; Reber, C.; Bélanger, S.; Beauchamp, A. L. *Inorg. Chem.* **1995**, *34*, 3851−3852. (c) Sartori, C.; Preetz, W. *Z. Naturforsch.* **1988**, *43a*, 239−247. (d) Winkler, J. R.; Gray, H. B. *Inorg. Chem.* **1985**, *24*, 346−355.
(7) (a) McMaster, J.; Carducci, M. D.; Yang, Y.-S.; Solomon, E. I.; Enemark, J. H. *Inorg. Chem.* **2001**, *40*, 687−702. (b) Baldas, J.; Heath, G. A.; Macgregor, S. A.; Moock, K. H.; Nissen, S. C.; Raptis, R. G. *J. Chem. Soc., Dalton Trans.* **1998**, 2303−2314. (c) Carducci, M. D.; Brown, C.; Solomon, E. I.; Enemark, J. H. *J. Am. Chem. Soc.* **1994**, *116*, 11856-11868. (d) Sabel, D. M.; Gewirth, A. A. *Inorg. Chem.* **1994**, *33*, 148−156. (e) Brewer, J. C.; Thorp, H. H.; Slagle, K. M.; Brudvig, G. W.; Gray, H. B. *J. Am. Chem. Soc.* **1991**, *113*, 3171−3173. (f) Deeth, R. J. *J. Chem. Soc., Dalton Trans.* **1991**, 1895−1900. (g) Deeth, R. J. *J. Chem. Soc., Dalton Trans.* **1991**, 1467−1477. (h) Collison, D. *J. Chem. Soc., Dalton Trans.* **1990**, 2999−3006. (i) Collison, D. *J. Chem. Soc., Dalton Trans.* **1989**, 1−4. (j) Sartori, C.; Preetz, W. *Z. Anorg. Allg. Chem.* **1988**, *565*, 23−33. (k) Sunil, K. K.; Harrison, J. F.; Rogers, M. T. *J. Chem. Phys.* **1982**, *76*, 3087−3097. (l) Winkler, J. R.; Gray, H. B. *Comments Inorg. Chem.* **1981**, *1*, 257−263. (m) Collison, D.; Gahan, B.; Garner, C. D.; Mabbs, F. E. *J. Chem. Soc., Dalton Trans.* **1980**, 667−674. (n) Weber, J.; Garner, C. D. *Inorg. Chem.* **1980**, *19*, 2206−2209. (o) Hill, L. H.; Howlader, N. C.; Mabbs, F. E.; Hursthouse, M. B.; Malik, K. M. A. *J. Chem. Soc., Dalton Trans.* **1980**, 1475−1481. (p) Garner, C. D.; Hill, L. H.; Mabbs, F. E.; McFadden, D. L.; McPhail, A. T. *J. Chem. Soc., Dalton Trans.* **1977**, 1202−1207. (q) Garner, C. D.; Hill, L. H.; Mabbs, F. E.; McFadden, D. L.; McPhail, A. T. *J. Chem. Soc., Dalton Trans.* **1977**, 853−858. (r) Garner, C. D.; Kendrick, J.; Lambert, P.; Mabbs, F. E.; Hillier, I. H. *Inorg. Chem.* **1976**, *15*, 1287−1291. (s) Garner, C. D.; Hillier, I. H.; Kendrick, J.; Mabbs, F. E. *Nature* **1975**, *258*, 138−139. (t) Al-Mowali, A. H.; Porte, A. L. *J. Chem. Soc., Dalton Trans.* **1975**, 50−55. (u) Garner, C. D.; Hillier, I. H.; Mabbs, F. E.; Guest, M. F. *Chem. Phys. Lett.* **1975**, *32*, 224−226. (v) Wentworth, R. A. D.; Piper, T. S. *J. Chem. Phys.* **1964**, *41*, 3884−3889. (w) Gray, H. B.; Hare, C. R. *Inorg. Chem.* **1962**, *1*, 363−386.
(8) (a) Filippou, A. C.; Philippopoulos, A. I.; Portius, P.; Neumann, D. U. *Angew. Chem., Int. Ed.* **2000**, *39*, 2778−2781. (b) Yam, V. W.-W.; Pui, Y.-L.; Wong, K. M.-C.; Cheung, K.-K. *Inorg. Chim. Acta* **2000**, *300*−*302*, 721−732. (c) Lehnert, N.; Tuczek, F. *Inorg. Chem.* **1999**, *38*, 1671−1682. (d) Kim, W.-S.; Kaltsoyannis, N. *Inorg. Chem.* **1998**, *37*, 674−678. (e) Vyboishchikov, S. F.; Frenking, G. *Chem. Eur. J.* **1998**, *4*, 1439−1448. (f) Cotton, F. A.; Feng, X. *Inorg. Chem.* **1996**, *35*, 4921−4925. (g) Yam, V. W.-W.; Tam, K.-K. *J. Chem. Soc., Dalton Trans.* **1994**, 391−392. (h) Kaltsoyannis, N. *J. Chem. Soc., Dalton Trans.* **1994**, 1391−1400. (i) Paradis, J. A.; Wertz, D. W.; Thorp, H. H. *J. Am. Chem. Soc.* **1993**, *115*, 5308−5309. (j) Vining, W. J.; Neyhart, G. A.; Nielson, S.; Sullivan, B. P. *Inorg. Chem.* **1993**, *32*, 4214−4217. (k) Manna, J.; Geib, S. J.; Hopkins, M. D. *J. Am. Chem. Soc.* **1992**, *114*, 9199−9200.
(9) Manna, J.; Gilbert, T. M.; Dallinger, R. F.; Geib, S. J.; Hopkins, M. D. *J. Am. Chem. Soc.* **1992**, *114*, 5870−5872.
(10) Isovitsch, R. A.; Beadle, A. S.; Fronczek, F. R.; Maverick, A. W. *Inorg. Chem.* **1998**, *37*, 4258−4264.
(11) Bendix, J.; Bøgevig, A. *Inorg. Chem.* **1998**, *37*, 5992−6001.
(12) Cotton, F. A.; Schmid, G. *Inorg. Chem.* **1997**, *36*, 2267−2278.
(13) Neyhart, G. A.; Seward, K. J.; Boaz, J.; Sullivan, B. P. *Inorg. Chem.* **1991**, *30*, 4486-4488.
(14) Wigley, D. E. *Prog. Inorg. Chem.* **1994**, *42*, 239−482.
(15) Mayr, A.; Ahn, S. *Adv. Transition Met. Coord. Chem.* **1996**, *1*, 1−103.
(16) Churchill, M. R.; Wasserman, H. J.; Turner, H. W.; Schrock, R. R. *J. Am. Chem. Soc.* **1982**, *104*, 1710−1716.
(17) Parkin, G. *Prog. Inorg. Chem.* **1998**, *47*, 1−165.
(18) Filippou, A. C.; Portius, P.; Philippopoulos, A. I. *Organometallics* **2002**, *21*, 653−661.

no)ethane). It is found that the energies and intensities of the fingerprint n → π^* ligand-field transitions of the phosphine derivatives deviate significantly from the predictions of an electronic structure model that assumes these ions possess effective tetragonal symmetry, in contrast to the standard approximation for such compounds. A general theoretical model is developed to explain the excited-state energies of structurally distorted complexes from the standpoint of the splitting of the degenerate orbitals and states and their associated one- and two-electron energy terms. The implications of these findings for understanding the electronic spectra of complexes with related excited states are discussed.

Experimental Section

General Procedures. HPLC-grade solvents, stored under nitrogen in stainless steel cylinders, were purified by passing them under nitrogen pressure through a stainless steel system consisting of either two 4.5 in. × 24 in. (1 gal) columns of activated A2 alumina (acetonitrile, diethyl ether, dichloromethane, and THF) or one column of activated A2 alumina and one column of activated BASF R3-11 catalyst (toluene).[19] The compounds $[MoO(dmpe)_2Cl]Cl$,[20] $[MoO(CNBu^t)_4Cl][BPh_4]$,[10] and $MoO(PMe_3)_3Cl_2$[21] were prepared according to standard procedures. FT-Raman spectra were recorded of solid samples in sealed NMR tubes at 1 cm^{-1} resolution with 1064-nm excitation using previously described instrumentation and procedures.[22] Frequencies were calibrated against an external indene reference. Emission spectra were recorded using a Spex Fluorolog II spectrophotometer equipped with a Xenon lamp and an R406 photomultiplier tube. Polycrystalline samples were mounted in copper-containing grease on a copper plate in a cryostat. Spectra were corrected for instrument response using standard procedures.[23] Elemental analyses were performed by Midwest Microlab, LLC.

$[MoO(PMe_3)_4Cl][PF_6]$. To a stirred, room-temperature solution of $MoO(PMe_3)_3Cl_2$ (0.41 g, 1.00 mmol) in THF (15 mL) under nitrogen were added PMe_3 (0.2 mL, 1.93 mmol) and KPF_6 (0.19 g, 1.03 mmol). The reaction mixture was stirred for 12 h, during which a purple precipitate formed. The volatile components were removed in vacuo, and the resulting purple solid was washed with toluene (5 × 10 mL), dried, and extracted with CH_2Cl_2 (15 mL). Filtration of this solution through Celite followed by removal of the volatile components under vacuum yielded 0.49 g (82% yield) of product. Slow vapor diffusion of diethyl ether into a concentrated CH_2Cl_2 solution of the salt afforded purple needle-shaped crystals suitable for X-ray diffraction studies. Anal. for $C_{12}H_{36}ClF_6MoOP_5$ Calcd (Found): C 24.16 (24.34), H 6.08 (6.01). ^1H NMR (CD_2Cl_2, 500.13 MHz): δ 1.73 (virtual t). $^{13}C\{^1H\}$ NMR (CD_2Cl_2, 125.77 MHz): δ 18.1 (m). $^{31}P\{^1H\}$ NMR (CD_2Cl_2, 212.46 MHz): δ −10.0 (s, *P*Me_3), −144.5 (sep, *P*F_6).

Single-Crystal X-ray Diffraction Studies. X-ray crystal structures were determined using a Bruker AXS SMART APEX diffractometer with graphite-monochromated Mo Kα ($\lambda = 0.71073$ Å) radiation. Crystals were attached to fine glass fibers with either Fluorolube or epoxy and placed in a cold N_2 stream for data collection. Initial cell constants were calculated using approximately 1000 reflections taken from data frames collected at either three or four values of ϕ (0°, 90°, 180°, and, in some cases, 270°). The data were processed using SAINT (v 6.02) and were corrected for X-ray absorption using SADABS (v 2.01 or 2.03). All computer programs used in the structure solution and refinement are contained in the SHELXTL (v 5.1) program suite. Crystal data and data collection and refinement parameters are set out in Table 1.

Table 1. Crystallographic Data for $[MoOL_4Cl][X]$ Complexes

param	$[MoO(CNBu^t)_4Cl][BPh_4]$	$[MoO(PMe_3)_4Cl][PF_6]$	$[MoO(dmpe)_2Cl]Cl\cdot 5H_2O$
chemical formula	$C_{44}H_{56}BClMoN_4O$	$C_{12}H_{36}ClF_6MoOP_5$	$C_{12}H_{42}Cl_2MoO_6P_4$
fw	799.13	596.65	573.18
color	purple	purple	purple
cryst syst	monoclinic	monoclinic	orthorhombic
space group	*I*2/*a* (No. 15)	$P2_1/c$ (No. 14)	*Pbcm* (No. 57)
a, Å	14.227(3)	7.5442(5)	9.4515(10)
b, Å	21.291(4)	27.7006(19)	11.9016(12)
c, Å	14.626(3)	12.1325(8)	23.214(2)
β, deg	90.925(4)	95.1850(10)	90
V, Å^3	4429.8(14)	2524.4(3)	2611.2(5)
ρ_{calcd}, g cm^{-3}	1.198	1.570	1.458
Z	4	4	4
μ (cm^{-1})	3.92	9.87	9.74
T, K	100	100	100
GOF	1.179	0.995	1.183
R1 [$I > 2\sigma(I)$]	0.063	0.037	0.042
wR2 [$I > 2\sigma(I)$]	0.161	0.077	0.121
R1 (all data)	0.067	0.046	0.043
wR2 (all data)	0.164	0.081	0.121

Direct methods were employed to determine the positions of heavy atoms; all remaining non-hydrogen atoms were located from subsequent difference Fourier syntheses and refined using full-matrix least-squares methods. Idealized hydrogen-atom positions and thermal parameters were derived from the atoms to which they are bonded (except for those of the interstitial water molecules of $[MoO(dmpe)_2Cl]Cl\cdot 5H_2O$, for which no hydrogen atoms were refined). The final cycles of refinement for each structure used anisotropic thermal parameters for all non-hydrogen atoms, except where noted.

$[MoO(CNBu^t)_4Cl][BPh_4]$. Unit-cell parameters, systematic absences, intensity statistics, and successful structure refinement allowed assignment of the space group of $[MoO(CNBu^t)_4Cl][BPh_4]$ as $I4_1/a$ at 300 K[24] and *I*2/*a* at 100 K. Direct methods revealed that the cation is orientationally disordered, such that the O-atom position of one orientation is nearly superimposed with the Cl-atom position of the other orientation and the Mo-atom positions are symmetrically displaced from the midpoint of the O/Cl and Cl/O positions. A similar form of disorder was reported for $[MoO(CNMe)_4Cl][I_3]$[25] and is common for $M(E)L_nX_{5-n}$ complexes.[26] Positions for the O, Mo, Cl, and ligating C atoms of both orientations were refined, each at one-half occupancy (because the two orientations are related by symmetry at 300 K in the $I4_1/a$ unit cell). Additionally, the *tert*-butyl groups of two isocyanide ligands are disordered over two positions; this was modeled by setting the site occupancy of each position to one-half.

$[MoO(PMe_3)_4Cl][PF_6]$. Initial refinement of the structure suggested that the cation is orientationally disordered in a manner

(19) Pangborn, A. B.; Giardello, M. A.; Grubbs, R. H.; Rosen, R. K.; Timmers, F. J. *Organometallics* **1996**, *15*, 1518−1520.
(20) Carmona, E.; Galindo, A.; Guille-Photin, C.; Sánchez, L. *Polyhedron* **1988**, *7*, 1767−1771.
(21) (a) Carmona, E.; Galindo, A.; Sánchez, L.; Nielson, A. J.; Wilkinson, G. *Polyhedron* **1984**, *3*, 347−352. (b) Butcher, A. V.; Chatt, J. *J. Chem. Soc. A.* **1970**, *16*, 2652−2656.
(22) John, K. D.; Miskowski, V. M.; Vance, M. A.; Dallinger, R. F.; Geib, S. J.; Wang, L. C.; Hopkins, M. D. *Inorg. Chem.* **1998**, *37*, 6858−6873.
(23) Parker, C. A.; Rees, W. T. *Analyst* **1960**, *85*, 587−600.
(24) Full details are available in the Supporting Information.
(25) Lam, C. T.; Lewis, D. L.; Lippard, S. J. *Inorg. Chem.* **1976**, *15*, 989−991.
(26) Parkin, G. *Chem. Rev.* **1993**, *93*, 887−911.

similar to $[MoO(CNBu^t)_4Cl][BPh_4]$. Because electron density attributable to O or Cl atoms of the second orientation was not observed, the disorder was modeled by refinement of a second Mo atom position (Mo′) only. The total occupancy of the Mo/Mo′ sites was constrained to unity, and the positions were refined using a shared free variable that describes relative site occupancies based on observed electron density; site-occupancy factors of 0.891 (Mo) and 0.109 (Mo′) were found for the two orientations. Attempts to refine the position of Mo′ using anisotropic displacement parameters led to poor refinement of Mo, so the final refinement of Mo′ used isotropic thermal parameters.

Polarized Single-Crystal Electronic Absorption Spectroscopy. Single-crystal electronic absorption spectra were recorded with an Aviv-Cary 14DS spectrophotometer. Samples were mounted on Pyrex plates and masked with copper-containing grease. Crystals of $[MoO(dmpe)_2Cl]Cl\cdot 5H_2O$ were overlaid with glass coverslips to prevent efflorescence. Samples were cooled using an APD Cryogenics Inc. closed-cycle helium cryostat. Sample temperatures were measured (±0.2 K) with a silicon-diode thermocouple. Polarized spectra were recorded by inserting a rotatable Glan-Thompson polarizer in the beam path approximately 12 cm in front of the sample block. Optical densities were maintained at reasonable levels (<2.5) by inserting neutral density screens in the reference beam path. Raw crystal spectra were corrected by subtraction of background spectra collected through the crystal mask and Pyrex plate at appropriate polarizer settings. Wavelengths were calibrated against a standard of $Ho(ClO_4)_3$ in perchloric acid solution.[27] Miller indices of single-crystal samples were determined using an X-ray diffractometer. Molecular-axis polarized spectra were obtained from polarized single-crystal spectra as outlined later. For all compounds, the isotropic spectra calculated from the molecular-axis spectra at 300 K closely matched the solution spectra.[24] Franck−Condon analyses of band profiles were performed with a computer program[28a,b] that used as input Franck−Condon factors calculated with the program LEVEL (v 7.4).[28c]

$[MoO(CNBu^t)_4Cl][BPh_4]$. Large crystals of the salt in the shape of rectangular pyramids were obtained by slow evaporation of acetonitrile solutions under nitrogen. The Mo≡O bond axes (molecular *z* axes; Figure 1) are ∥*c* of the $I4_1/a$ unit cell (∥*b* of the $I2/a$ unit cell at 100 K), which is normal to the base of the crystal pyramid; thus, crystals were mounted on an edge and polished with alumina powder to yield an undeveloped face that contains this axis. Optical microscopy of this polished section revealed it to be highly dichroic, passing from dark purple (⊥*z*) to nearly colorless (∥*z*) upon rotation of the electric vector.

$[MoO(PMe_3)_4Cl][PF_6]$. Slow vapor diffusion of diethyl ether into a concentrated CH_2Cl_2 solution of the salt under nitrogen afforded large needle-shaped crystals elongated along the *a* axis ($P2_1/c$ unit cell). Polishing undeveloped {*h*0*l*} faces proved to be difficult, so polarized spectra were recorded on the naturally developed $\{0\bar{1}1\}$ and $\{0\bar{1}0\}$ faces. The extinction directions of the $\{0\bar{1}1\}$ face are located +10° (pale purple) and −80° (dark purple) from the needle axis, and those of the $\{0\bar{1}0\}$ face occur at +28° (pale purple) and −62° (red) from the needle axis; the rotation angles refer to the direction of rotation from the +*a* axis toward the +*c* axis. No wavelength dependence of the extinction directions was observed for either face. Molecular-axis polarized spectra derived from the crystal spectra using the coordinate system shown in Figure 1 show negative absorbances in the ∥*z* spectrum, suggesting that the principal absorption directions are not properly defined by this coordinate system; spectra derived using a new coordinate system in which the *x* and *z* axes are rotated 5° about the *y* axis from their idealized positions lack these features and are presented here.[24] The relationships between the crystal spectra and the rotated molecular axes are given by the equations shown later. The molecular axes of molecules related by the *c* glides or the 2_1 axes have different projections on the extinction directions in the $\{0\bar{1}1\}$ face; these projections are averaged in the equations for $I(+10°)$ and $I(-80°)$. The molecular-axis spectra were derived using standard methods for cases where none of the crystal spectra are common to both faces.[29] Because of the crystallographic disorder of the $[MoO(PMe_3)_4Cl]^+$ ion, the projections of the molecular *x* and *y* axes on the extinction directions are scrambled in proportion to the site occupancies (9:1). Moreover, the two orientations of the chromophore were found to give rise to spectra in which corresponding features are shifted from each other by ca. 300 cm^{-1}.[24] Because it is impossible to separate the contributions to the molecular-axis spectra from the minor and major orientations, the equations correspond to a hypothetical ordered crystal.

$$I(+10°) = 0.115I_x + 0.072I_y + 0.813I_z$$

$$I(-80°) = 0.739I_x + 0.201I_y + 0.060I_z$$

$$I(+28°) = 0.063I_x + 0.019I_y + 0.918I_z$$

$$I(-62°) = 0.037I_x + 0.955I_y + 0.008I_z$$

$[MoO(dmpe)_2Cl]Cl\cdot 5H_2O$. Slow evaporation of aqueous solutions of $[MoO(dmpe)_2Cl]Cl$ in air afforded large diamond-shaped plates developed along the {001} plane (*Pbcm* unit cell), with the *a* and *b* axes approximately bisecting the obtuse and acute angles of this face, respectively. Polarized absorption spectra were recorded along the lattice vectors of both this face and the {100} face, which was obtained by polishing ⊥*a* on thick crystals. This latter face was found to be strongly dichroic, appearing dark purple (∥*c*) and red (∥*b*). The crystal spectra are related to the molecular axes (Figure 1) by the following equations:

$$I_a = 0.702I_x + 0.298I_z$$

$$I_b = 0.298I_x + 0.702I_z$$

$$I_c = I_y$$

Results and Discussion

Theoretical Considerations. The electronic spectra of d^1 and d^2 *trans*-MOL_4X, *trans*-MOL_4, and *trans*-MO_2L_4 complexes are typically described in the context of the orbital energy diagram shown in Figure 2a, which illustrates that the degenerate d_{xz} and d_{yz} orbitals are destabilized relative to the d_{xy} orbital as a result of their strong π^*(MO) character.[5] For d^2 complexes, the large splitting (Δ_π) between the d_{xy} and (d_{xz}, d_{yz}) orbitals produces a $^1A_1$ [$(d_{xy})^2$] ground state. The lowest-energy ligand-field transition is [$(d_{xy})^2 \rightarrow (d_{xy})^1$-

(27) Weidner, V. R.; Mavrodineanu, R.; Mielenz, K. D.; Velapoldi, R. A.; Eckerle, K. L.; Adams, B. *J. Res. Natl. Bur. Stand. (U.S.)* **1985**, *90*, 115−125.

(28) (a) Da Re, R. E. Unpublished results. (b) Stoner, T. C.; Miskowski, V. M.; Hopkins, M. D. *Comput. Chem.* **1993**, *17*, 327−329. (c) Le Roy, R. J. *LEVEL 7.4: A Computer Program for Solving the Radial Schrödinger Equation for Bound and Quasibound Levels*; University of Waterloo Chemical Physics Research Report CP-642 R3, 2001. The source code and manual for this program may be obtained from the Computer Programs link on the www site http://leroy.uwaterloo.ca.

(29) Hitchman, M. A. *J. Chem. Soc., Faraday Trans. 2* **1976**, *72*, 54−62.

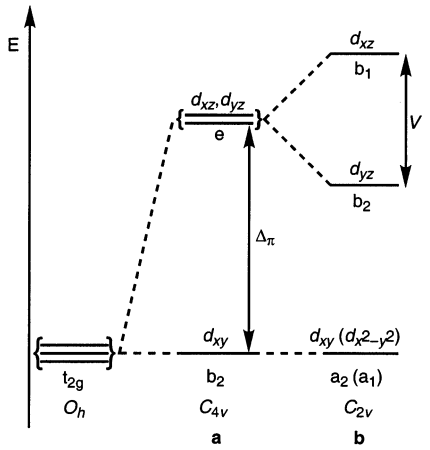

Figure 2. Relative energies of the t_{2g}-parentage d orbitals for MOL_4X complexes: (a) C_{4v} symmetry; (b) C_{2v} symmetry. The magnitudes of V and Δ_π are not drawn to scale. For b, the orbitals and Mulliken symbols in parentheses are those for structural type **IIb** that differ from those for structural type **IIa**.

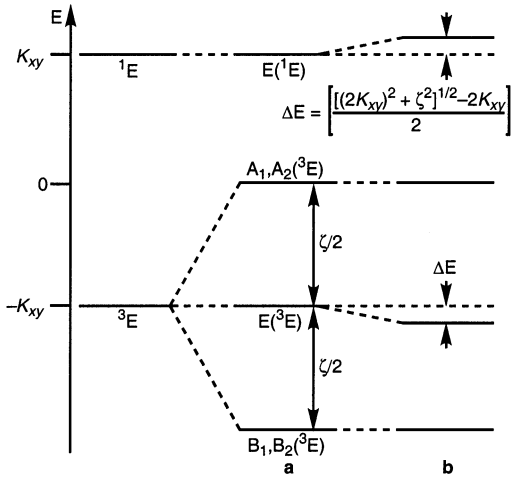

Figure 3. Effect of spin−orbit coupling on the energies of the ^{1}E and ^{3}E n → π^* excited states (adapted from ref 5): (a) first-order spin−orbit coupling, where ζ is the spin−orbit coupling constant; (b) second-order spin−orbit coupling, showing the mixing between the E(^{1}E) and E(^{3}E) states.

(d_{xz}, d_{yz})[1]]; this electronic transition is frequently denoted "n → π^*" on the basis of the symmetries of the d_{xy} and (d_{xz}, d_{yz}) orbitals relative to the MO bond(s).[5] The ^{1}E and ^{3}E excited states produced by this transition are separated in energy by the two-electron term $2K_{xy}$ ($K_{xy} = 3B + C$ for the $(t_{2g})^2$ configuration). Under the influence of spin−orbit coupling, illustrated in Figure 3, the 6-fold-degenerate ^{3}E state is split into three sublevels, and the E(^{1}E) and E(^{3}E) spin−orbit states are mixed. The mixing of the E-symmetry states shifts their energies from first-order values and enhances the intensity of the formally spin-forbidden A_1-($^1A_1$) → E(^{3}E) transition (vide infra).

Structural distortions of MOL_4X complexes that lift the tetragonal symmetry may change this picture significantly because they lead to formal splittings of the degenerate (e symmetry) orbitals and electronic states. Distortions that reduce the symmetry of an MOL_4X complex from C_{4v} to C_{2v}, such as those resulting in the inequivalent OML or LML bond angles found in structural types **IIa** and **IIb** (Figure 1), split the d_{xz} and d_{yz} π^*(M≡O) orbitals, as shown in Figure

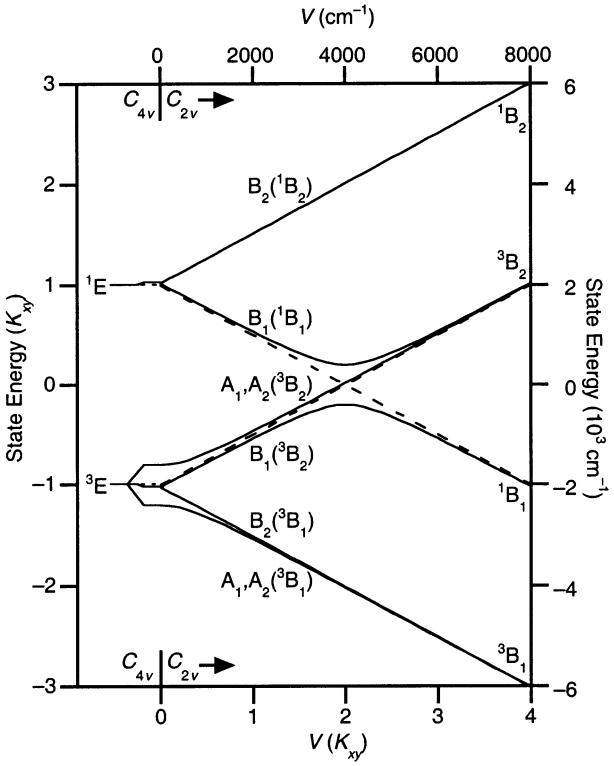

Figure 4. Effects of spin−orbit coupling and the splitting of the π^*(M≡O) orbitals on the energies of the ^{1}E and ^{3}E n → π^* excited states with $2K_{xy}$ = 4000 cm^{-1} and ζ = 800 cm^{-1}. The state labels are given for a complex of structural type **IIa** (see Figure 1); for structural type **IIb**, the labels B_1 and B_2 are interchanged. Labels for the spin−orbit levels in the tetragonal limit ($V = 0$) are given in Figure 3. The dashed lines denote the first-order energies of the $^1B_1$ and $^3B_2$ states.

2b.[30] We adopt the (arbitrary) convention that d_{yz} and d_{xz} are stabilized and destabilized, respectively, relative to their energies under C_{4v} symmetry by an energy denoted $V/2$.

The degeneracies of the ^{1}E and ^{3}E excited states produced by the n → π^* ligand-field transition (Figure 3) are also lifted by distortions from C_{4v} to C_{2v} symmetry. The results of a ligand-field calculation that quantifies the effects of the d_{xz}/d_{yz} orbital splitting on the energies of these excited states are shown in Figure 4, in which a value of the spin−orbit coupling constant that is reasonable for Mo(IV) (ζ[Mo(IV) free ion] = 920 cm^{-1})[31] has been assumed. A key point to be taken from this calculation is that states of B_1 and B_2 symmetry behave differently as $V \rightarrow 2K_{xy}$. The $B_1(^1B_1)$ and $B_1(^3B_2)$ states converge to produce an avoided crossing centered at $V = 2K_{xy}$, meaning that they are strongly mixed in this region, whereas the $B_2(^1B_2)$ and $B_2(^3B_1)$ states diverge as V increases, so mixing between them decreases continuously with increasing V. For $V \gg 2K_{xy}$, the large separation between like-symmetry excited states yields the simple ordering of energy levels expected for strongly inequivalent n → π^*_{xz} and n → π^*_{yz} transitions.[32]

The splitting of the E-symmetry excited states under C_{2v} symmetry has important implications for the intensities of the n → π^* absorption bands, in addition to the consequences

(30) For compounds of type **IIb**, the molecular coordinate system is different from that of **IIa** (Figure 1), which interchanges some orbital and state labels. For simplicity, the HOMO will be designated d_{xy} (as for **IIa**) in this section.

already described for the transition energies. For the n → $\pi^*_{xz,yz}$ transitions of a C_{4v}-symmetry complex, the band attributable to the formally spin-forbidden $A_1(^1A_1) \rightarrow E(^3E)$ transition steals intensity from that of the spin-allowed $A_1(^1A_1) \rightarrow E(^1E)$ transition according to eq 1:[33]

$$f_{OT} = f_{OS}\frac{E_T - E_O}{E_S - E_O}\frac{\left(\frac{\zeta}{2}\right)^2}{(\Delta E_{ST})^2} \quad (1)$$

where f_{OT} and f_{OS} are the oscillator strengths of the triplet and singlet bands, respectively, E_O, E_T, and E_S are the energies of the $A_1(^1A_1)$, $E(^3E)$, and $E(^1E)$ states, respectively, $\frac{\zeta}{2}$ is the off-diagonal spin−orbit matrix element that couples the $E(^3E)$ and $E(^1E)$ states,[5] and ΔE_{ST} is the energy difference between the first-order $E(^1E)$ and $E(^3E)$ states ($2K_{xy}$, Figure 3). Under C_{2v} symmetry, the increasing mixing between B_1 spin−orbit states and decreasing mixing between B_2 spin−orbit states as $V \rightarrow 2K_{xy}$ (Figure 4) should profoundly affect these intensities. Specifically, $\Delta E_{ST} = 2K_{xy} - V$ for the $B_1(^1B_1)$ (n → π^*_{yz}) and $B_1(^3B_2)$ (n → π^*_{xz}) states, so intensity transfer between these bands should increase dramatically, relative to a C_{4v} chromophore, as $V \rightarrow 2K_{xy}$. Conversely, the $B_2(^1B_2)$ (n → π^*_{xz}) and $B_2(^3B_1)$ (n → π^*_{yz}) states are increasingly energy factored as $V \rightarrow 2K_{xy}$ ($\Delta E_{ST} = 2K_{xy} + V$), so intensity transfer between these bands should be comparatively small.

The magnitudes of the effects described here depend, for a given compound, upon the extent of the structural distortion and the symmetries and strengths of its M−L interactions. In the following section, the structural distortions of $[MoOL_4Cl]^+$ ions are classified using X-ray crystallography. The effects of these distortions on the bonding and spectra of the $[MoOL_4Cl]^+$ ions are then investigated through analysis of their n → π^* electronic transitions, which are assigned using polarized single-crystal spectroscopy.

X-ray Diffraction Studies and Vibrational Spectroscopy. The molecular structures of the *trans*-$[MoOL_4Cl]^+$ ions were investigated by X-ray crystallography and vibrational spectroscopy in order to establish their point and crystallographic symmetries and to investigate the effects of the ancillary ligands on the Mo≡O bond distance. The crystal structures of the $[MoOL_4Cl]^+$ ions (L = $CNBu^t$, PMe_3, $^1/_2$-dmpe) are shown in Figure 5, and selected metrical data and MoO stretching frequencies are set out in Table 2. All ions possess pseudooctahedral structures in which the molybdenum atom is displaced slightly above the average plane of the equatorial ligating atoms, as is typical of $M(\equiv E)L_n$ complexes.[34] The bond distances and angles for $[MoO(dmpe)_2Cl]^+$, which is the only $[MoOL_4Cl]^+$ ion that is not disordered, lie within normal ranges.[35] Unfortunately, the crystallographic disorder of $[MoO(CNBu^t)_4Cl][BPh_4]$ and $[MoO(PMe_3)_4Cl][PF_6]$ prohibits quantitative structural analysis of these compounds; leading indicators of this are the

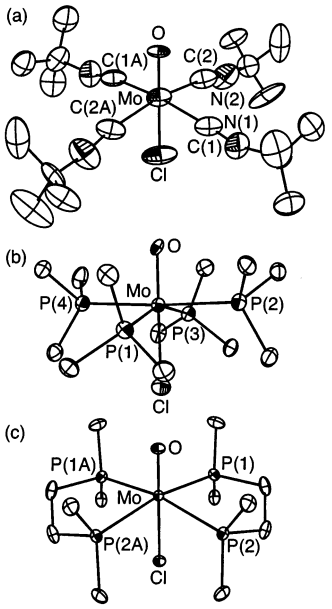

Figure 5. ORTEP drawings of $[MoOL_4Cl]^+$ ions (50% probability ellipsoids): (a) $[MoO(CNBu^t)_4Cl][BPh_4]$ (one orientation shown); (b) $[MoO(PMe_3)_4Cl][PF_6]$ (major orientation shown); (c) $[MoO(dmpe)_2Cl]Cl\cdot 5H_2O$. Hydrogen atoms are omitted for clarity.

Table 2. Molybdenum−Oxo Stretching Frequencies (cm^{-1}) and Selected Bond Lengths (Å) and Bond Angles (deg) for $[MoOL_4Cl][X]$Complexes

	$[MoO(CNBu^t)_4Cl][BPh_4]$[a]	$[MoO(PMe_3)_4Cl][PF_6]$[b]	$[MoO(dmpe)_2Cl]Cl\cdot 5H_2O$
ν(MoO)	952[c]	948	959[d]
Mo−O	1.758(17), 1.72(3)	1.737(3)	1.690(4)
Mo−Cl	2.410(12), 2.419(8)	2.5023(19)	2.5606(14)
Mo−L(1)	2.178(11), 2.154(12)	2.5494(11)	2.5106(10)
Mo−L(2)	2.176(12), 2.174(9)	2.5467(10)	2.4948(10)
Mo−L(3)	2.178(11), 2.154(12)[e]	2.5291(10)	2.4948(10)[f]
Mo−L(4)	2.176(12), 2.174(9)[e]	2.5448(10)	2.5106(10)[f]
O−Mo−Cl	180, 180	178.18(8)	177.89(14)
O−Mo−L(1)	94.1(2), 94.3(2)	102.32(8)	96.72(9)
O−Mo−L(2)	96.1(3), 96.6(2)	87.89(8)	97.79(9)
O−Mo−L(3)	94.1(2), 94.3(2)[e]	99.80(9)	97.79(9)[f]
O−Mo−L(4)	96.1(3), 96.6(2)[e]	88.84(8)	96.72(9)[f]
L(1)−Mo−L(2)	86.7(4), 88.0(4)	89.01(3)	79.42(3)
L(2)−Mo−L(3)	92.4(4), 91.0(4)[e]	90.01(3)	99.24(5)[f]
L(3)−Mo−L(4)	86.7(4), 88.0(4)[e]	93.26(3)	79.42(3)[f]
L(4)−Mo−L(1)	92.4(4), 91.0(4)[e]	89.00(3)	98.21(5)[f]

[a] Disordered 1:1 over two orientations; metrical data for both orientations given. [b] Disordered 9:1 over two orientations; metrical data given for the major-occupancy orientation. [c] Reference 10. [d] Datum for anhydrous $[MoO(dmpe)_2Cl]Cl$. [e] L(3) = C(1A) and L(4) = C(2A) (Figure 5a). [f] L(3) = P(2A) and L(4) = P(1A) (Figure 5c).

(31) Bendix, J.; Brorson, M.; Schäffer, C. E. *Inorg. Chem.* **1993**, *32*, 2838−2849.
(32) The model used to derive Figure 4 is incomplete because there is no requirement that nondegenerate n → π^*_{xz} and n → π^*_{yz} excited states be characterized by a single electron−electron repulsion energy K_{xy}. Ligand-field calculations that treat $K_1 \neq K_2$ (where K_1 and K_2 are the two-electron terms associated with the n → π^*_{xz} and n → π^*_{yz} excited states, respectively) are presented in the Supporting Information. The $K_1 \neq K_2$ case is treated as a small perturbation to the energies of the electronic states depicted in Figure 4 because, for the present compounds, $V \gg K_1 - K_2$.
(33) Ballhausen, C. J. *Introduction to Ligand Field Theory*; McGraw-Hill: New York, 1962; p 191.
(34) Nugent, W. A.; Mayer, J. M. *Metal−Ligand Multiple Bonds*; Wiley: New York, 1988; pp 157−158.
(35) (a) Owens, B. E.; Poli, R. *Acta Crystallogr.* **1992**, *C48*, 2137−2140. (b) The crystal structures of the BPh_4^- and PF_6^- salts of this ion are available as Supporting Information. The MoO bond distances for the three $[MoO(dmpe)_2Cl]^+$ ions fall within the 1.657−1.696 Å range for six-coordinate Mo(IV) monooxo complexes (19 entries in the Cambridge Structural Database, version 5.21 (April 2001)).

MoO and MoCl bond distances,[26] which are too long and too short, respectively, relative to those of $[MoO(dmpe)_2Cl]^+$ and expected values.

The crystallographic results indicate that the idealized point symmetries of the $[MoOL_4Cl]^+$ ions depend on the steric properties of the ancillary ligands in the expected way. The structure of $[MoO(CNBu^t)_4Cl]^+$, which is sterically uncrowded near the metal center, possesses idealized C_{4v} point symmetry (**I**, Figure 1).[36] The $[MoO(PMe_3)_4Cl]^+$ ion possesses approximate C_{2v} symmetry (**IIa**, Figure 1), with two trans phosphorus nuclei lying roughly at right angles to the Mo≡O moiety (∠OMoP ≅ 88°) and the other two significantly displaced below these (∠OMoP ≅ 100°) because of the steric repulsions among the phosphine methyl groups. The $[MoO(dmpe)_2Cl]^+$ ion possesses approximate C_{2v} symmetry (**IIb**, Figure 1), exhibiting a more regular arrangement of phosphorus nuclei relative to the Mo≡O bond (∠OMoP ≅ 97°) than does $[MoO(PMe_3)_4Cl]^+$, but strong distortions from tetragonal symmetry within the P_4 plane due to the steric constraints imposed by the ethylene backbone (∠PMoP ≅ 79° and 99° within and between the chelate rings, respectively). The crystallographic site symmetries of the $[MoOL_4Cl]^+$ ions are lower than their idealized point symmetries, being C_2 for $[MoO(CNBu^t)_4Cl][BPh_4]$, C_s for $[MoO(dmpe)_2Cl]Cl\cdot 5H_2O$, and C_1 for $[MoO(PMe_3)_4Cl][PF_6]$; the site symmetries are taken into account in the interpretation of the electronic spectra, but the idealized point symmetries are sufficient for explaining the major electronic differences among these compounds (vide infra).

The vibrational spectroscopic data indicate that neither these structural differences nor the natures of the ancillary ligands significantly influence the Mo≡O bond lengths of the $[MoOL_4Cl]^+$ ions. The Mo≡O stretching frequencies of these ions (Table 2) span a narrow range (948−959 cm^{-1}). A prior study of the vibrational spectra of the related complex $W(CH)(PMe_3)_4Cl$[37] established an empirical relationship between M≡E force constants and bond lengths for third-transition-series complexes. Although a quantitative relationship of this type has not been derived for complexes of the second transition series, application of that for the third-row complexes[37] to the data for $[MoOL_4Cl]^+$ suggests that the Mo≡O bond lengths of these ions probably differ by <0.01 Å, in agreement with the general picture for M≡O complexes.[38] Thus, the marked differences among the n → π^* electronic transitions of these ions (vide infra) cannot be attributed to gross differences in Mo≡O bond distance.

n → π^* Electronic Transitions of $[MoO(CNBu^t)_4Cl]^+$. The n → π^* electronic absorption bands of the $[MoO(CNBu^t)_4Cl]^+$ ion exhibit energies, intensities, polarizations, and vibronic structure that are consistent with the indication from the crystal structure of this ion that it should be a prototypical tetragonally symmetric MOL_4X chromophore.

(36) The statistical significance of the spread of OMoC (94.1(2)°, 96.1(3)°) and CMoC bond angles (86.7(4)°, 92.4(4)°) of $[MoO(CNBu^t)_4Cl]^+$ (Table 2) is uncertain, being tied to the unknown adequacy of the model for the disordered carbon-atom positions.
(37) Manna, J.; Dallinger, R. F.; Miskowski, V. M.; Hopkins, M. D. *J. Phys. Chem. B* **2000**, *104*, 10928−10939.
(38) Mayer, J. M. *Inorg. Chem.* **1988**, *27*, 3899−3903.

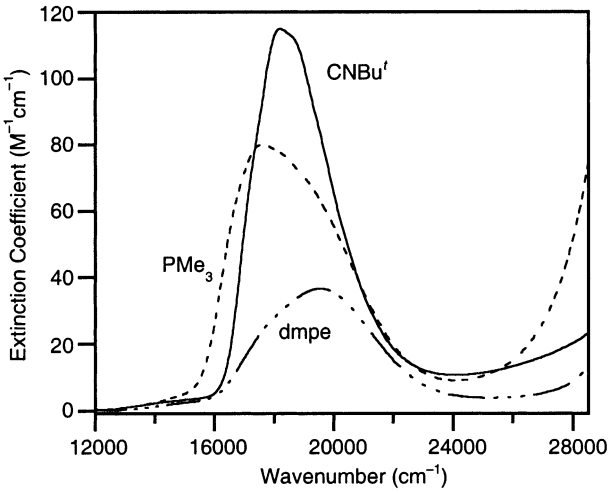

Figure 6. Electronic absorption spectra of $[MoOL_4Cl]^+$ ions in CH_2Cl_2 solution at 300 K in the region of the n → π^* ligand-field transition.

Table 3. Electronic Absorption Spectroscopic Data for $[MoOL_4Cl]^+$ Ions in CH_2Cl_2 Solution at 300 K

ion	λ_{max} (nm)	$\bar{\nu}_{max}$ (cm^{-1})	ϵ (M^{-1} cm^{-1})	f^a	fwhm (cm^{-1})
$[MoO(CNBu^t)_4Cl]^+$	549	18215	115[b]	1.8×10^{-3}	3200
$[MoO(PMe_3)_4Cl]^+$	568	17605	80	1.7×10^{-3}	4500
$[MoO(dmpe)_2Cl]^+$	512	19530	37	7.5×10^{-4}	4600

[a] Integrated over entire n → π^* band system. [b] Reference 10.

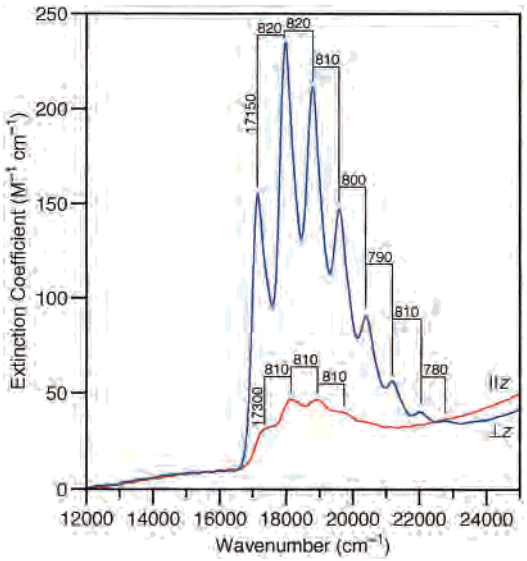

Figure 7. Polarized single-crystal electronic absorption spectra of $[MoO(CNBu^t)_4Cl][BPh_4]$ at 18 K.

In solution at room temperature, a weak (ϵ 115 M^{-1} cm^{-1}), relatively narrow (fwhm 3200 cm^{-1}) absorption band is observed at 18215 cm^{-1} (549 nm); this band is shown in Figure 6, where it is overlaid with those for the other $[MoOL_4Cl]^+$ ions (vide infra), and the band parameters are set out in Table 3. This band was assigned by Maverick and co-workers to the $^1A_1 \rightarrow {}^1E$ $[(d_{xy})^2 \rightarrow (d_{xy})^1(d_{xz}, d_{yz})^1]$ transition (denoted hereafter n → $\pi^*_{xz,yz}$) on the basis of molecular orbital considerations (Figure 2a).[10] The polarized single-crystal absorption spectra of $[MoO(CNBu^t)_4Cl][BPh_4]$, shown in Figure 7, confirm this assignment: the band exhibits strong ⊥z polarization ($I(\perp z)/I(\parallel z) \cong 5$), as expected

Table 4. Excited-State Configurations, Symmetries, and Molecular-Axis Polarizations of n → π^* Transitions of $[MoOL_4Cl]^+$ Ions[a]

transition	$[MoO(CNBu^t)_4Cl]^+$ $[(d_{xy})^1(d_{xz},d_{yz})^1]$	$[MoO(PMe_3)_4Cl]^+$ $[(d_{xy})^1(d_{xz})^1]$	$[MoO(PMe_3)_4Cl]^+$ $[(d_{xy})^1(d_{yz})^1]$	$[MoO(dmpe)_2Cl]^+$ $[(d_{x^2-y^2})^1(d_{xz})^1]$	$[MoO(dmpe)_2Cl]^+$ $[(d_{x^2-y^2})^1(d_{yz})^1]$
^{1}[n → π^*]	$E(^1E)$, ⊥z	$B_2(^1B_2)$, ∥y	$B_1(^1B_1)$, ∥x	$B_1(^1B_1)$, ∥x	$B_2(^1B_2)$, ∥y
^{3}[n → π^*]	$A_1(^3E)$, ∥z; $A_2(^3E)$, F	$A_1(^3B_2)$, ∥z	$A_1(^3B_1)$, ∥z	$A_1(^3B_1)$, ∥z	$A_1(^3B_2)$, ∥z
	$E(^3E)$, ⊥z	$B_1(^3B_2)$, ∥x	$B_2(^3B_1)$, ∥y	$B_2(^3B_1)$, ∥y	$B_1(^3B_2)$, ∥x
	$B_1(^3E)$, F; $B_2(^3E)$, F	$A_2(^3B_2)$, F	$A_2(^3B_1)$, F	$A_2(^3B_1)$, F	$A_2(^3B_2)$, F

[a] Transitions from the $A_1(^1A_1)$ ground states; F denotes a forbidden transition. The coordinate system for each complex is given in Figure 1. Orbital and excited-state orderings are depicted in Figures 2−4.

from the electric-dipole selection rules for the $^1A_1 \rightarrow {}^1E$ transition (Table 4). The nonzero intensity of the $^1A_1 \rightarrow {}^1E$ band in ∥z polarization, in which it is dipole forbidden, is vibronically induced. This interpretation is suggested by the observation that the vibronic features in the ∥z-polarized spectrum are blue-shifted relative to their counterparts in the ⊥z-polarized spectrum.

The principal structural distortion of the $[MoO(CNBu^t)_4Cl]^+$ ion in the ^1E excited state is elongation of the MoO bond, a finding that is consistent with the orbital character of the n → $\pi^*_{xz,yz}$ transition. In the ⊥z-polarized spectrum (Figure 7), well resolved vibronic structure is observed, with an average spacing of 810 cm^{-1}, that is assigned to the MoO stretching frequency of the ^1E excited state. This frequency is reduced relative to the ground state (952 cm^{-1}, Table 2), consistent with the reduction in the formal Mo−O bond order from 3 to 2.5 in the excited state. Franck−Condon analysis of this vibronic structure provides an excited-state elongation along the Mo−O stretching coordinate of $\Delta Q(MoO) = 0.09$ Å. This distortion is similar in magnitude to those calculated for the n → π^* excited states of other multiply metal−ligand bonded complexes.[6,39] Deconvolution of the vibronic bands indicates that at least one lower-frequency mode (⩽400 cm^{-1}) is also vibronically active, which is characterized by a small Huang−Rhys factor and, thus, small excited-state distortion. Vibronic activity of Mo−Cl and Mo−C modes, which are of the appropriate frequency to account for the additional vibronic intensity, would be unsurprising on the basis of the fact that vibronic structure attributable to metal−ancillary-ligand modes has been observed in the n → π^* bands of other d^2 chromophores.[6,39,40]

In addition to the $^1A_1 \rightarrow {}^1E$ (n → $\pi^*_{xz,yz}$) absorption band, a weak band system attributable to one or more spin−orbit components of the $^1A_1 \rightarrow {}^3E$ (n → $\pi^*_{xz,yz}$) transition is observed in spectra of solution (Figure 6) and single-crystal samples of $[MoO(CNBu^t)_4Cl][BPh_4]$. Shown in Figure 8 for this complex are an unpolarized absorption spectrum (15 K) of a thick crystal and the 0−0 band of the emission spectrum (14 K). The energy of the latter is identical (within experimental error) to that reported by Maverick and co-workers for a spectrum recorded at 77 K.[10] It was not possible to obtain polarization data for the triplet absorption band because it is extremely weak in polished crystal samples. However, the observation of vibronic spacings of ca. 800 cm^{-1} marks it clearly as an n → $\pi^*_{xz,yz}$ transition.

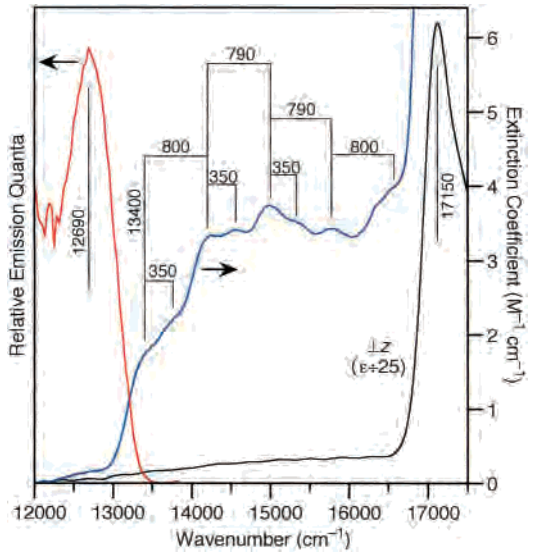

Figure 8. Electronic absorption and emission spectra of $[MoO(CNBu^t)_4Cl][BPh_4]$: (red) 0−0 band of the emission spectrum recorded of a polycrystalline sample at 14 K; (blue) unpolarized absorption spectrum recorded of a thick crystal (unknown face) at 15 K; (black) ⊥z-polarized single-crystal spectrum (from Figure 7).

The electronic transitions that are expected to give rise to absorption bands in this region are, in order of increasing energy, $A_1(^1A_1) \rightarrow B_1,B_2(^3E)$, $A_1(^1A_1) \rightarrow E(^3E)$, and $A_1(^1A_1) \rightarrow A_1,A_2(^3E)$ (Figure 3). The $A_1(^1A_1) \rightarrow B_1,B_2(^3E)$ transition is forbidden (Table 4). Because this transition should directly produce the emissive excited state, the lower limit for the origin of the corresponding absorption band is set by the position of the emission 0−0 band (12690 cm^{-1}). No distinct absorption features are observed in this region; in studies of $[OsNX_4]^-$ (X = Cl, Br) ions, the origin of the analogous absorption band was also found to be too weak to observe.[39] The $A_1(^1A_1) \rightarrow E(^3E)$ transition, which is expected to be the next highest in energy, is dipole allowed and gains intensity by the mixing between the $E(^3E)$ and $E(^1E)$ states (eq 1). The band originating at 13400 cm^{-1} is assigned to this transition. The 3750 cm^{-1} separation between the origins of the $A_1(^1A_1) \rightarrow E(^1E)$ and $A_1(^1A_1) \rightarrow E(^3E)$ bands is reasonable for a Mo(IV) singlet−triplet energy gap (vide infra), which supports this assignment. A second set of vibronic features with a ca. 800 cm^{-1} spacing lie 350 cm^{-1} to higher energy of these peaks. These could correspond to a second vibronically active mode of the $A_1(^1A_1) \rightarrow E(^3E)$ band, similar in frequency to that present in the $^1A_1 \rightarrow {}^1E$ band, or to the $A_1(^1A_1) \rightarrow A_1,A_2(^3E)$ band. We disfavor the

(39) (a) Hopkins, M. D.; Miskowski, V. M.; Gray, H. B. *J. Am. Chem. Soc.* **1986**, *108*, 6908−6911. (b) Cowman, C. D.; Trogler, W. C.; Mann, K. R.; Poon, C. K.; Gray, H. B. *Inorg. Chem.* **1976**, *15*, 1747−1751.

(40) (a) Collison, D.; Garner, C. D.; Mabbs, F. E.; King, T. J. *J. Chem. Soc., Dalton Trans.* **1981**, 1820−1824. (b) Collison, D.; Garner, C. D.; Mabbs, F. E.; Salthouse, J. A.; King, T. J. *J. Chem. Soc., Dalton Trans.* **1981**, 1812−1819.

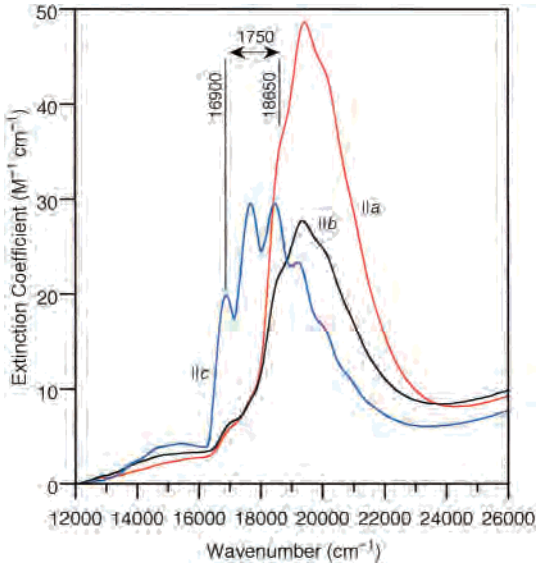

Figure 9. Polarized single-crystal electronic absorption spectra of [MoO(dmpe)$_2$Cl]Cl·5H$_2$O at 22 K.

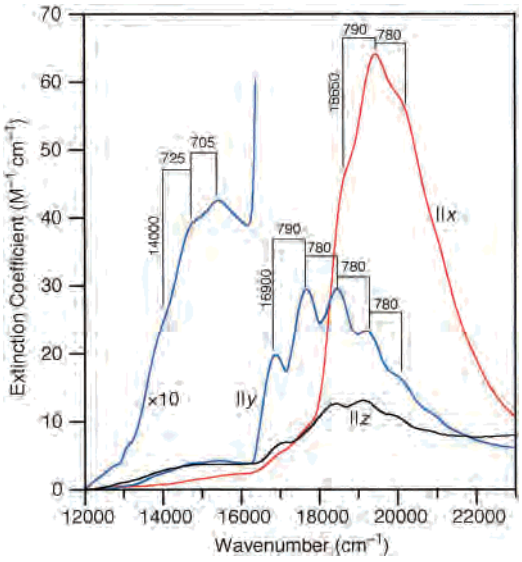

Figure 10. Molecular-axis polarized electronic absorption spectra of [MoO(dmpe)$_2$Cl]Cl·5H$_2$O at 22 K.

latter interpretation because the $A_1(^1A_1) \rightarrow A_1,A_2(^3E)$ band should be much less intense than the $A_1(^1A_1) \rightarrow E(^3E)$ band. The $A_1(^1A_1) \rightarrow A_1,A_2(^3E)$ band is presumably buried within the $A_1(^1A_1) \rightarrow E(^3E)$ band envelope.

n → *π Electronic Transitions of [MoO(dmpe)$_2$Cl]$^+$.** The n → π^* electronic absorption band system of the [MoO(dmpe)$_2$Cl]$^+$ ion is considerably more complex than that of [MoO(CNBu^t)$_4$Cl]$^+$. The n → π^* absorption band of this ion in room-temperature solution is shown in Figure 6, and the band parameters are set out in Table 3. Strikingly, the band for [MoO(dmpe)$_2$Cl]$^+$ ($\bar{\nu}_{max}$ 19530 cm^{-1}, λ_{max} 512 nm, fwhm 4600 cm^{-1}) is 40% broader than that for [MoO(CNBu^t)$_4$Cl]$^+$ and exhibits a distinct shoulder, whereas the band for the latter is comparatively symmetrical in shape.

The polarized single-crystal absorption spectra of [MoO(dmpe)$_2$Cl]Cl·5H$_2$O at 22 K reveal that the broad band observed in the solution spectrum is the result of two overlapping electronic transitions.[41] These spectra, shown in Figure 9, exhibit two prominent, vibronically structured bands with different polarizations in the region of the n → π^* band observed in solution: one band (E_{0-0} 16900 cm^{-1}) appears in the ||*c*-polarized spectrum, and the other (E_{0-0} 18650 cm^{-1}) is evident in the ||*a*- and ||*b*-polarized spectra. There is also a weak band system centered at ca. 15000 cm^{-1}.

Resolution of these data into molecular-axis polarized spectra, shown in Figure 10, allows assignment of the absorption bands to specific orbital transitions (Table 4). The band with the origin at 16900 cm^{-1} is strongly ||*y*-polarized, which indicates an assignment of $^1A_1 \rightarrow {}^1B_2$ [$(d_{x^2-y^2})^2 \rightarrow (d_{x^2-y^2})^1(d_{yz})^1$] (denoted hereafter n → π^*_{yz}). The nonzero intensity of this band in ||*x*- and ||*z*-polarizations, in which it is dipole forbidden, is attributed to vibronic coupling on the basis that it decreases significantly upon cooling from 300 to 22 K.[24] The higher-energy absorption (E_{0-0} 18650 cm^{-1}) exhibits strong ||*x*-polarization and is assigned as $^1A_1 \rightarrow {}^1B_1$ [$(d_{x^2-y^2})^2 \rightarrow (d_{x^2-y^2})^1(d_{xz})^1$] (denoted n → π^*_{xz}). Thus, the distortion of the equatorial ligand field in this complex has resulted in an appreciable splitting of the d_{xz} and d_{yz} orbitals.

Franck−Condon analysis of the vibronic structure observed in the $^1A_1 \rightarrow {}^1B_2$ (n → π^*_{yz}) and $^1A_1 \rightarrow {}^1B_1$ (n → π^*_{xz}) bands indicates that the distortion of the MoO bond in these two nondegenerate excited states (ΔQ(MoO) = 0.09 Å) is similar to that in the $^1A_1 \rightarrow {}^1E$ (n → $\pi^*_{xz,yz}$) excited state of [MoO(CNBu^t)$_4$Cl]$^+$. Vibronic spacings of ca. 790 cm^{-1}, corresponding to the excited-state MoO stretching frequency, are discerned for both bands; this is reduced from the ground-state value of 959 cm^{-1} (Table 2). Thus, the M−L orbital interactions responsible for splitting the d_{xz} and d_{yz} orbitals of [MoO(dmpe)$_2$Cl]$^+$ do not strongly affect their MoO π-antibonding character.

The molecular-axis polarized spectra of [MoO(dmpe)$_2$Cl]Cl·5H$_2$O also exhibit weak bands attributable to spin-forbidden n → π^* electronic transitions. The spectra (Figure 10) exhibit a weakly structured feature at ca. 15000 cm^{-1} with mixed ||*y*- and ||*z*-polarization, suggesting it is composed of overlapping bands arising from two transitions. The ||*y*-polarized component is assigned to the $A_1(^1A_1) \rightarrow B_2(^3B_1)$ (n → π^*_{xz}) transition; the 4650 cm^{-1} energy gap between the origin of this band (E_{0-0} = 14000 cm^{-1}, based on deconvolution) and its singlet counterpart $^1A_1 \rightarrow {}^1B_1$ (n → π^*_{xz}) is concordant with a Mo(IV) singlet−triplet gap (vide infra). The ||*z*-polarized component is assigned to a transition to one of the A_1-symmetry n → π^* excited states. The fact that it is nearly identical in energy with the $A_1(^1A_1) \rightarrow B_2(^3B_1)$ (n → π^*_{xz}) band suggests that it be assigned to the $A_1(^1A_1) \rightarrow A_1(^3B_1)$ (n → π^*_{xz}) transition rather than the $A_1(^1A_1) \rightarrow A_1(^3B_2)$ (n → π^*_{yz}) transition, on the basis of the energy-level diagram in Figure 4. The $A_1(^1A_1) \rightarrow B_1(^3B_2)$ (n → π^*_{yz}) transition is not observed for this compound, but an extremely weak band ($\epsilon \sim 0.2$) is observed at ca. 13300 cm^{-1} in the unpolarized spectrum of a thick crystal of the

(41) Polarized single-crystal spectra for [MoO(dmpe)$_2$Cl][BPh$_4$] were also studied; these data are available in the Supporting Information. The data support the conclusions presented for [MoO(dmpe)$_2$Cl]Cl·5H$_2$O.

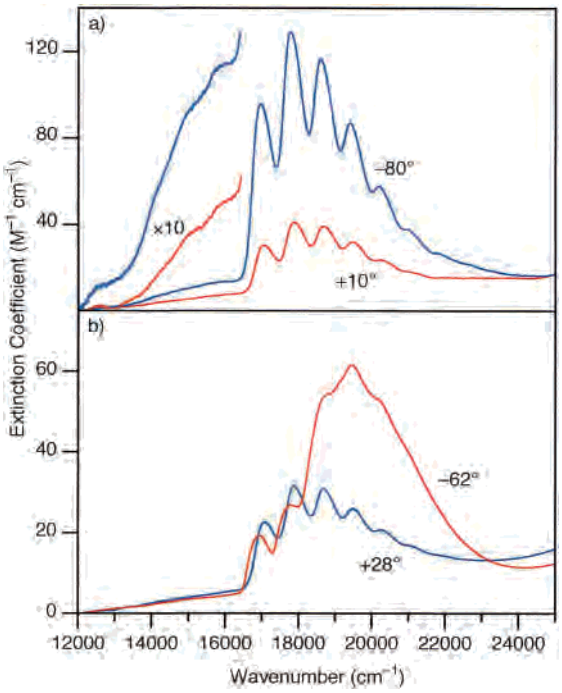

Figure 11. Polarized single-crystal electronic absorption spectra of [MoO(PMe$_3$)$_4$Cl][PF$_6$] at 18 K: (a) {0$\bar{1}$1} face (the ×10 expanded traces were recorded on a thicker crystal at 15 K); (b) {0$\bar{1}$0} face.

related salt [MoO(dmpe)$_2$Cl][BPh$_4$];[41] the ca. 4000 cm^{-1} separation between this band and the origin of the A$_1$(^{1}A$_1$) → B$_2$(^{1}B$_2$) (n → π^*_{yz}) band of this salt (E_{0-0} = 17300 cm^{-1}) makes this assignment reasonable. On the basis of these data, it is estimated that the origin of the A$_1$(^{1}A$_1$) → B$_1$(^{3}B$_2$) (n → π^*_{yz}) band lies near 12850 cm^{-1} for [MoO(dmpe)$_2$Cl]Cl·5H$_2$O.

n → π^* Electronic Transitions of [MoO(PMe$_3$)$_4$Cl]$^+$. The n → π^* electronic absorption band system of [MoO(PMe$_3$)$_4$Cl]$^+$ exhibits characteristics similar to those found for [MoO(dmpe)$_2$Cl]$^+$. As shown in Figure 6, the n → π^* band envelope of this ion in solution is considerably broader than that of [MoO(CNBu^t)$_4$Cl]$^+$ and exhibits a distinct shoulder on the high-energy flank. These observations suggest that the C_{2v}-symmetry ligand field of [MoO(PMe$_3$)$_4$Cl]$^+$, like that of the [MoO(dmpe)$_2$Cl]$^+$ ion, splits the degeneracy of the d$_{xz}$ and d$_{yz}$ orbitals, giving rise to two ^{1}[n → π^*] transitions.

The polarized single-crystal absorption spectra of [MoO(PMe$_3$)$_4$Cl][PF$_6$], shown in Figure 11, confirm that this chromophore possesses two ^{1}[n → π^*] transitions, which give rise to the vibronically structured bands with origins at 16950 and ca. 18700 cm^{-1}. The molecular-axis polarized spectra (Figure 12) allow assignment of the lower-energy band (||x-polarized) to the ^{1}A$_1$ → ^{1}B$_1$ [(d$_{xy}$)^2 → (d$_{xy}$)^1(d$_{yz}$)^1] transition (n → π^*_{yz}) and the higher-energy band (||y-polarized) to the ^{1}A$_1$ → ^{1}B$_2$ [(d$_{xy}$)^2 → (d$_{xy}$)^1(d$_{xz}$)^1] transition (n → π^*_{xz}).[42] The vibronic structure observed in both bands is attributable to the MoO stretching mode, exhibiting average vibronic

(42) The ||y-polarized spectrum also shows features that arise from the crystallographic disorder of the [MoO(PMe$_3$)$_4$Cl]$^+$ ion. A detailed analysis of these features, the interpretation of which is not germane to the subject of this paper, is provided in the Supporting Information.

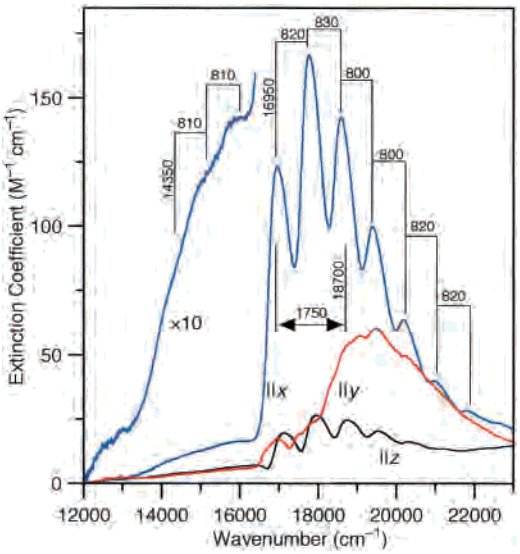

Figure 12. Molecular-axis polarized electronic absorption spectra of [MoO(PMe$_3$)$_4$Cl][PF$_6$] at 18 K.

spacings of 815 cm^{-1} for the lower-energy band and ca. 800 cm^{-1} for the higher-energy band; these frequencies are reduced from the ground-state MoO stretching frequency (948 cm^{-1}). Franck−Condon analysis of the ^{1}A$_1$ → ^{1}B$_1$ band provides ΔQ(MoO) = 0.09 Å, which is similar to those determined for the n → π^* excited states of [MoO(CNBu^t)$_4$Cl]$^+$ and [MoO(dmpe)$_2$Cl]$^+$. The spectra of [MoO(PMe$_3$)$_4$Cl][PF$_6$] also exhibit weak bands that are attributable to one or more ^{3}[n → π^*] transitions. The absorption between 13500 and 16500 cm^{-1} ($\epsilon \sim 10$) is predominantly ||x-polarized but shows nonzero intensity in ||y- and ||z-polarization, because of either the crystallographic disorder of the [MoO(PMe$_3$)$_4$Cl]$^+$ ion or contributions from overlapping bands. Assignment of this feature to A$_1$(^{1}A$_1$) → B$_1$(^{3}B$_2$) (n → π^*_{xz}) is suggested by the ||x-polarization and the reasonable 4350 cm^{-1} separation between its origin (E_{0-0} = 14350 cm^{-1}) and that of ^{1}A$_1$ → ^{1}B$_2$ (n → π^*_{xz}). No other bands in this region could be straightforwardly assigned.

Analysis. The electronic spectra of the [MoOL$_4$Cl]$^+$ ions show unequivocally that the nature of the n → π^* excited states and, thus, the electronic structure of the MoO bond depend on the geometry of the equatorial ligands. Specifically, the spectra of the C_{2v}-symmetry ions [MoO(dmpe)$_2$Cl]$^+$ and [MoO(PMe$_3$)$_4$Cl]$^+$ each exhibit two ^{1}[n → π^*] ligand-field bands, indicative of a splitting of the d$_{xz}$ and d$_{yz}$ π^*(MoO) orbitals, whereas the spectrum of C_{4v}-symmetry [MoO(CNBu^t)$_4$Cl]$^+$ shows a single ^{1}[n → π^*] band. Moreover, the intensities of these bands (and of their spin-forbidden counterparts) vary dramatically among this series of ions. The theoretical treatments outlined earlier (Figures 3 and 4) allow the spectroscopic data to be reduced to a set of one- and two-electron parameters (V, K_{xy}, Δ_π) that afford insight into the differences among the electronic structures of these ions.

The [MoO(CNBu^t)$_4$Cl]$^+$ ion provides spectroscopic benchmarks for understanding the spectra of the [MoO(dmpe)$_2$Cl]$^+$ and [MoO(PMe$_3$)$_4$Cl]$^+$ ions. Importantly, the observation of a single ^{1}[n → π^*] band in the electronic absorption spectra

Table 5. Ligand-Field Parameters (cm^{-1}) for $[MoOL_4Cl][X]$ Complexes[a]

param	$[MoO(CNBu^t)_4Cl][BPh_4]$	$[MoO(dmpe)_2Cl]Cl·5H_2O$[b]	$[MoO(PMe_3)_4Cl][PF_6]$[c]
V	0	1400−1560	1360−1500
K_{xy}	1790−1880		
K_1		2220−2300	2060−2200
K_2		1900−2020	1740−1820

[a] The ranges of V and K_{xy} (or K_1 and K_2) correspond to agreement between experimental and calculated transition energies of ±50 cm^{-1}; the value of ζ was taken to be 500−1000 cm^{-1}. [b] The calculated ranges of V, K_1, and K_2 for $[MoO(dmpe)_2Cl][BPh_4]$ are similar to those for this salt (see the Supporting Information). [c] The energy of onset of the red absorption edge of the electronic spectrum was used as an estimate for the energy of the $A_1(^1A_1) \rightarrow B_2(^3B_1)$ transition (Figure 4), which could not be straightforwardly assigned.

of $[MoO(CNBu^t)_4Cl]^+$ indicates that the d_{xz} and d_{yz} orbitals are degenerate ($V = 0$), consistent with effective C_{4v} point symmetry for this ion. Therefore, the relative excited-state energies can be analyzed in the context of the simple state diagram shown in Figure 3. Because only two of the four expected $n \rightarrow \pi^*$ transition energies are spectroscopically established, neither of which (for a second-row metal ion) is strongly dependent on the magnitude of spin−orbit coupling (ζ), a range for K_{xy} is calculated on the basis of the assumption of a chemically reasonable range of ζ (500−1000 cm^{-1}; ζ[Mo(IV) free ion] = 920 cm^{-1}).[31] Fitting of the relative energies of the $E(^1E)$ and $E(^3E)$ excited states (within ± 50 cm^{-1}) yields K_{xy} = 1790−1880 cm^{-1} (Table 5). Although no literature values of K_{xy} for Mo(IV) are available for comparison, the calculated range lies below that derived for Mo(III) from the $^4A_{2g} \rightarrow {}^2E_g, {}^2T_{1g}$ transitions of $[MoX_6]^{3-}$ (X = Cl, Br) ions (energy = $3K_{xy}$;[5] K_{xy} = 3100−3200 cm^{-1}).[43] The fact that K_{xy} is reduced for $[MoO(CNBu^t)_4Cl]^+$ is undoubtedly the result of covalent Mo−O and Mo−C bonding, which quenches two-electron terms.[5,44] From the values of K_{xy} and ζ, one can conclude that the energies of the $E(^1E)$ and $E(^3E)$ excited states are little perturbed from their first-order values (ΔE < 75 cm^{-1} in Figure 3b).

The observation of two $^1[n \rightarrow \pi^*]$ electronic absorption bands for the $[MoO(dmpe)_2Cl]^+$ and $[MoO(PMe_3)_4Cl]^+$ ions indicates that the d_{xz} and d_{yz} orbitals are nondegenerate ($V \neq 0$). Interpreting the transition energies of these ions requires the theoretical picture shown in Figure 4. Ranges of V and K_{xy} were established for these ions by fitting the relative energies of the B_1- and B_2-symmetry states. For $[MoO(dmpe)_2Cl]Cl·5H_2O$, relatively poor agreement between calculated and experimental energies ($\geqslant$225 cm^{-1}) for the B_1 and B_2 states was obtained unless different two-electron terms were used for the $[(d_{x^2-y^2})^1(d_{xz})^1]$ (K_1) and $[(d_{x^2-y^2})^1(d_{yz})^1]$ (K_2) electron configurations.[32] This is not unreasonable, in terms of the nephelauxetic effect of the phosphine ligands, because the degeneracy of the d_{xz} and d_{yz} orbitals must be lifted by differing interactions with phosphine orbitals (vide infra). Allowing for this splitting of K_{xy} dramatically improves the agreement ($\leqslant$50 cm^{-1}) between the calculated and experimental relative energies. The splitting between the d_{xz} and d_{yz} orbitals is found to be V = 1400−1560 cm^{-1}, with K_1 = 2220−2300 cm^{-1} for $[(d_{x^2-y^2})^1(d_{xz})^1]$ and K_2 = 1900−2020 cm^{-1} for $[(d_{x^2-y^2})^1(d_{yz})^1]$ (Table 5). Analysis of the excited-state energies of $[MoO(PMe_3)_4Cl]^+$ is less straightforward, because fewer $n \rightarrow \pi^*$ bands were identified, but comparable values of V, K_1, and K_2 are obtained (Table 5).

It is important to note that the gross differences between the spectra of $[MoO(CNBu^t)_4Cl]^+$ and the $[MoO(PR_3)_4Cl]^+$ ions are a consequence of both the splitting of the d_{xz} and d_{yz} orbitals ($V \neq 0$) and of K_{xy} ($K_1 \neq K_2$) in the phosphine derivatives. This point is emphasized by the fact that the separation between their $^1[n \rightarrow \pi^*_{xz}]$ and $^1[n \rightarrow \pi^*_{yz}]$ bands ($\Delta E_{0-0} \cong$ 1750 cm^{-1}) is larger than the calculated d_{xz}/d_{yz} splitting ($V \cong$ 1500 cm^{-1}), which requires $K_1 > K_2$.[24] It is logical to attribute both the splitting of the d_{xz} and d_{yz} orbitals and of K_{xy} of the phosphine derivatives to the structurally imposed inequivalence of their $Mo(d_{xz})$−P and $Mo(d_{yz})$−P interactions.

What are the specific M−L orbital interactions responsible for lifting the degeneracy of the d_{xz} and d_{yz} orbitals in $[MoO(dmpe)_2Cl]^+$ and $[MoO(PMe_3)_4Cl]^+$? While the exact natures and strengths of these interactions are best deduced by quantum-mechanical calculations, which are beyond the scope of this work, calculations based on simple geometrical (angular-overlap) considerations provide some insight into this question. For $[MoO(dmpe)_2Cl]^+$, angular-overlap calculations predict $E(d_{yz}) > E(d_{xz})$ for the dmpe ligands acting exclusively as σ-donors and $E(d_{xz}) > E(d_{yz})$ for them acting exclusively as π-acceptors toward these orbitals.[45] Although interactions of both types undoubtedly influence the energies of the π^*(MoO) orbitals, the spectroscopically observed $E(d_{xz}) > E(d_{yz})$ ordering suggests that Mo → dmpe π-back-bonding is principally responsible for splitting the d_{xz} and d_{yz} orbitals for this ion. For $[MoO(PMe_3)_4Cl]^+$, angular-overlap calculations predict $E(d_{xz}) > E(d_{yz})$ because of a cooperative destabilization of d_{xz} by σ-donation and stabilization of d_{yz} by π-back-bonding of the PMe_3 ligands,[46] consistent with the relative energies of the $n \rightarrow \pi^*_{xz}$ and $n \rightarrow \pi^*_{yz}$ bands of this ion. Regardless of the specific Mo−PR_3 interaction(s) involved in splitting the d_{xz} and d_{yz} orbitals, however, the strong π^*(MoO) character of these orbitals is not appreciably altered. This point is emphasized by the fact that the excited-state distortions of the MoO bond are similar for all three $[MoOL_4Cl]^+$ ions (ΔQ(MoO) = 0.09 Å). Consistent with this, the values of Δ_π calculated[5] from the state energies and values of K_{xy} (or K_1 and K_2) lie in the narrow range 19000−21000 cm^{-1} for all three ions.

The splitting of the d_{xz} and d_{yz} orbitals of $[MoO(dmpe)_2Cl]^+$ and $[MoO(PMe_3)_4Cl]^+$ has important implications for the spin purity of the $n \rightarrow \pi^*$ excited states and the intensities of the associated absorption bands. The fact that $V \cong 0.7K$ ($K \equiv {}^1/_2(K_1 + K_2)$) for $[MoO(dmpe)_2Cl]^+$ and $[MoO(PMe_3)_4Cl]^+$ means that these chromophores lie between the limits of

(43) Smith, P. W.; Wedd, A. G. *J. Chem. Soc. A.* **1970**, 2447−2454.
(44) Lever, A. B. P. *Inorganic Electronic Spectroscopy*, 2nd ed.; Elsevier: Amsterdam, 1984; Chapter 9.

(45) $E(d_{xz}) = 0.0802(e_\sigma(dmpe)) + 1.653(-e_\pi(dmpe))$; $E(d_{yz}) = 0.1155(e_\sigma(dmpe)) + 2.347(-e_\pi(dmpe))$.
(46) $E(d_{xz}) = 0.2482(e_\sigma(PMe_3)) + 1.669(-e_\pi(PMe_3))$; $E(d_{yz}) = 0.0143(e_\sigma(PMe_3)) + 1.990(-e_\pi(PMe_3))$.

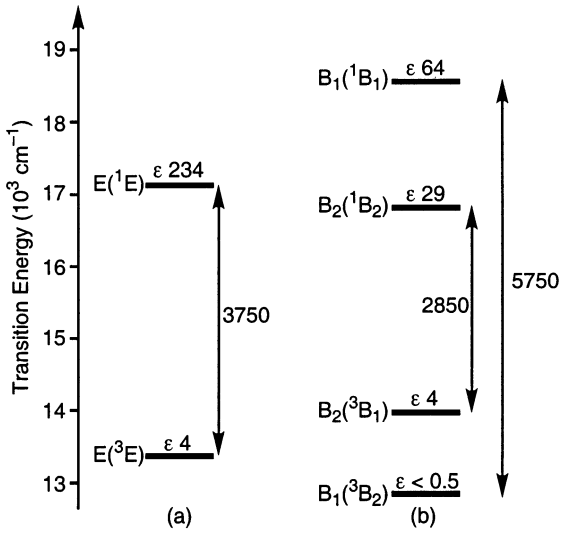

Figure 13. Transition energies and extinction coefficients (n → π^*) of $[MoOL_4Cl]^+$ ions: (a) $[MoO(CNBu^t)_4Cl][BPh_4]$; (b) $[MoO(dmpe)_2Cl]Cl\cdot 5H_2O$. Energy separations between states are given in cm^{-1}.

tetragonal symmetry, for which the mixing of singlet and triplet states is small (e.g., $[MoO(CNBu^t)_4Cl]^+$), and of the avoided crossing at $V = 2K_{xy}$ (Figure 4), at which point the converged B-symmetry singlet and triplet states are completely mixed. Consequently, there should be a significant redistribution of absorption intensities between singlet−singlet and singlet−triplet n → π^* absorption bands of the $[MoO(PR_3)_4Cl]^+$ ions relative to what is anticipated for a C_{4v}-symmetry $[MoOL_4Cl]^+$ ion (eq 1). The n → π^* bands of $[MoO(CNBu^t)_4Cl]^+$ ($\Delta E_{ST} = 3750$ cm^{-1}) provide reference points for this prediction: the intensity of the $A_1(^1A_1)$ → $E(^3E)$ band (ϵ 4) is less than 2% that of the $A_1(^1A_1)$ → $E(^1E)$ band (ϵ 234). For $[MoO(dmpe)_2Cl]^+$, by comparison, the smaller separation between the $B_2(^3B_1)$ (n → π^*_{xz}) and $B_2(^1B_2)$ (n → π^*_{yz}) states ($\Delta E_{ST} = 2850$ cm^{-1}) gives rise to stronger mixing between them; the intensity of the $A_1(^1A_1)$ → $B_2(^3B_1)$ band is nearly 15% that of the $A_1(^1A_1)$ → $B_2(^1B_2)$ band. In contrast, the $B_1(^3B_2)$ (n → π^*_{yz}) and $B_1(^1B_1)$ (n → π^*_{xz}) states of $[MoO(dmpe)_2Cl]^+$ are widely separated ($\Delta E_{ST} \cong 5800$ cm^{-1}); as a consequence of this energy factoring, the $A_1(^1A_1)$ → $B_1(^3B_2)$ (n → π^*_{yz}) band is vanishingly weak in the spectra of $[MoO(dmpe)_2Cl]^+$.[47] These observations are summarized in Figure 13. The n → π^* bands of $[MoO(PMe_3)_4Cl]^+$ behave similarly to those of $[MoO(dmpe)_2Cl]^+$: the energetic proximity of the $B_1(^3B_2)$ (n → π^*_{xz}) and $B_1(^1B_1)$ (n → π^*_{yz}) states ($\Delta E_{ST} = 2600$ cm^{-1}) enhances the intensity of the $A_1(^1A_1)$ → $B_1(^3B_2)$ (n → π^*_{xz}) band, whereas the much larger separation between the coupled $B_2(^3B_1)$ (n → π^*_{yz}) and $B_2(^1B_2)$ (n → π^*_{xz}) states ($\Delta E_{ST} > 6000$ cm^{-1}) renders the $A_1(^1A_1)$ → $B_2(^3B_1)$ (n → π^*_{yz}) band too weak to be observed in these spectra. Thus, the energetically outlying states within the n → π^* manifold of states are well described by their conventional spin−orbit designations; the $B_2(^3B_1)$ (n → π^*_{xz}) and $B_2(^1B_2)$ (n → π^*_{yz}) states of $[MoO(dmpe)_2Cl]^+$ and the $B_1(^3B_2)$ (n → π^*_{xz}) and $B_1(^1B_1)$ (n → π^*_{yz}) states of $[MoO(PMe_3)_4Cl]^+$, in contrast, are not.

Relevance to Related Complexes and Excited States. The data and analysis presented here call into question the validity of approximate electronic structure models that ascribe functional tetragonal symmetry to the general class of $ME(PR_3)_4X$ and $ME_2(PR_3)_4$ chromophores. Specifically, the lower symmetries of these compounds can result in significant splittings of the d_{xz} and d_{yz} π^*(ME) orbitals (in the present case, by ca. 10% of Δ_π) and of the two-electron term K_{xy}, resulting in two n → π^* transitions and strong mixing between certain singlet and triplet excited states.[48] Although this has not been previously recognized for this class of compounds, the reported solution electronic spectra of several such compounds appear to manifest these effects.[11−13] The spectra for third-transition-series metal complexes of these general types are expected to be more complicated than those for metal complexes of the second transition series, because of their greater spin−orbit coupling; preliminary investigations of the analogous ion $[WO(dmpe)_2Cl]^+$ confirm this prediction.[49] Naturally, the spectrum of any d^2 MEL_4, $MEL_2L'_2$, or $MEL_2L'_2X$ complex with approximate C_{2v} symmetry, of which numerous examples are known, can be expected to be similarly affected; the theoretical treatment presented in Figure 4 also applies to these chromophores.

With respect to computational endeavors directed at understanding the electronic structures of $ME(PR_3)_4X$ and $ME_2(PR_3)_4$ complexes, the findings presented here suggest that caution is required in approximating the geometry at the metal center. It is common practice to assess the quality of such calculations by comparing the calculated and observed molecular structures and vibrational frequencies of the compound in question. For the $[MoOL_4Cl]^+$ ions of the present study, the fingerprint MoO force constant is essentially independent of the geometry of the ancillary ligands; it would doubtless be the case that calculations on a C_{4v}-symmetry model compound such as $[MoO(PH_3)_4Cl]^+$ would reproduce the MoO bond distances and force constants of $[MoO(dmpe)_2Cl]^+$ and $[MoO(PMe_3)_4Cl]^+$ while missing the splittings of the d_{xz} and d_{yz} orbitals and of K_{xy} that are the origins of the spectroscopic complexity of these ions.

The results and conclusions described here can also be extended to $M(ER)L_4X$ chromophores in which the splitting of the d_{xz} and d_{yz} orbitals derives not from a structural distortion of the L ligands but from an R group on the multiply bonded ligand with a single π face. Common examples of such compounds include triply bonded phenylimido (E = NPh)[14] and benzylidyne (or phenyl carbyne; E = CPh)[15] derivatives, as well as compounds with double bonds such as metal−alkylidene (or carbene; E = CR_2) complexes. Spectroscopic data are available for metal−benzylidyne complexes of the type $M(CPh)L_4X$; the absorption bands arising from the n → π^*_{xz} transition (where π^*_{xz}

(47) The $A_1(^1A_1)$ → $B_2(^3B_1)$ n → π^*_{xz} band is 15 times more intense than the $A_1(^1A_1)$ → $B_1(^3B_2)$ n → π^*_{yz} band in spectra recorded of thick crystals of $[MoO(dmpe)_2Cl][BPh_4]$ (see the Supporting Information for details).

(48) The exception to this would be $ME_2(PR_3)_4$ compounds with D_{2d} symmetry, under which the d_{xz} and d_{yz} orbitals remain degenerate.

(49) Da Re, R. E.; Hopkins, M. D. Manuscript in preparation.

is stabilized relative to π^*_{yz} due to mixing with π^* orbitals on the phenyl ring) are strongly red-shifted from the corresponding n → π^* bands of M(CR)L_4X (R = H, alkyl),[9,50] suggesting that $V = 6-9 \times 10^3$ cm^{-1}. At such large orbital splittings ($V \gg 2K_{xy}$), mixing between like-symmetry spin−orbit states is dramatically reduced, and as a result, the $^3B_1$ and $^3B_2$ states are expected to exhibit little or no zero-field splitting (Figure 4). Thus, the extent of spin-singlet character mixed into the $^3[n \rightarrow \pi^*_{xz}]$ excited states is anticipated to be very small, and the intensities of absorption bands arising from transitions to these excited states should be weak relative to the $^3[n \rightarrow \pi^*]$ bands of MEL_4X and M(ER)L_4X complexes with effective symmetries that more closely approximate ideal tetragonal symmetry (i.e., $V \ll 2K_{xy}$). Preliminary investigations of W(CH)(dmpe)$_2$X and W(CPh)(dmpe)$_2$X complexes (X = halide) reveal that the much larger splitting between the d_{xz} and d_{yz} orbitals of the latter results in a significant decrease in mixing between like-symmetry singlet- and triplet-parentage states, as evidenced by the comparatively weak $^3[n \rightarrow \pi^*_{xz}]$ bands of W(CPh)-(dmpe)$_2$X relative to the $^3[n \rightarrow \pi^*]$ bands of W(CH)-(dmpe)$_2$X.[51]

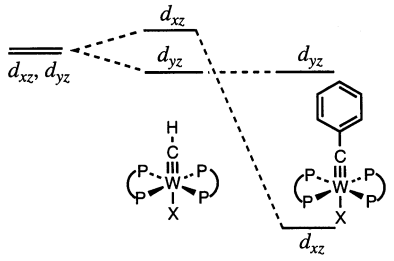

As a final point, we note that the theoretical treatment given here can be applied to other excited states generated by transitions between δ- and π-symmetry orbitals. Specifically, the $\pi \rightarrow$ n transitions of d^0 *trans*-MEL_4X complexes,[52] the $[(d_{xz},d_{yz})^2 \rightarrow (d_{xz},d_{yz})^1(d_{x^2-y^2})^1]$ transitions of d^8 ML_4 chromophores, and the $[(\delta^*)^2 \rightarrow (\delta^*)^1(\pi^*)^1]$ transitions of d^5−d^5 multiply metal−metal bonded complexes[53] each generate ^{1}E- and ^{3}E-derived excited states that are subject to the perturbations due to structural distortions described herein.

Acknowledgment. We thank Vince Miskowski for helpful discussions, Ian Steele and Joe Pluth for assistance with indexing crystal faces, Larry Henling for helpful discussions concerning the crystal structure of [MoO(CNBu^t)$_4$Cl][BPh$_4$], and Professor Don Levy for bringing the program LEVEL to our attention. This research was supported by the National Science Foundation (Grant CHE 9700451).

Supporting Information Available: X-ray crystallographic data for [MoO(CNBu^t)$_4$Cl][BPh$_4$] (300 and 100 K), [MoO(dmpe)$_2$Cl]-Cl·5H$_2$O, [MoO(PMe$_3$)$_4$Cl][PF$_6$], [MoO(dmpe)$_2$Cl][BPh$_4$], and [MoO(dmpe)$_2$Cl][PF$_6$], available in CIF format. Ligand-field calculations treating inequivalent two-electron terms for n → π^*_{xz} and n → π^*_{yz} excited states. Polarized single-crystal and molecular-axis electronic absorption spectra of [MoO(dmpe)$_2$Cl][BPh$_4$] (at 300 and 16 K). Details concerning the polarized spectra of [MoO-(PMe$_3$)$_4$Cl][PF$_6$]. Polarized and calculated isotropic spectra (300 K) of the [MoOL_4Cl][X] compounds. This material is available free of charge via the Internet at http://pubs.acs.org.

IC020565R

(50) (a) Bocarsly, A. B.; Cameron, R. E.; Rubin, H.-D.; McDermott, G. A.; Wolff, C. R.; Mayr, A. *Inorg. Chem.* **1985**, *24*, 3976−3978. (b) Bocarsly, A. B.; Cameron, R. E.; Mayr, A.; McDermott, G. A. In *Photochemistry and Photophysics of Coordination Compounds*; Yersin, H., Vogler, A., Eds.; Springer-Verlag: Berlin, 1987; pp 213−216.
(51) Da Re, R. E. Unpublished results.
(52) (a) Williams, D. S.; Korolev, A. V. *Inorg. Chem.* **1998**, *37*, 3809−3819. (b) Williams, D. S.; Thompson, D. W.; Korolev, A. V. *J. Am. Chem. Soc.* **1996**, *118*, 6526−6527. (c) Heinselman, K. S.; Hopkins, M. D. *J. Am. Chem. Soc.* **1995**, *117*, 12340−12341.
(53) The isomorphic relationship between the $[(\delta^*)^2 \rightarrow (\delta^*)^1(\pi^*)^1]$ electronic states of D_{4h}- and D_{2d}-symmetry multiply metal−metal bonded complexes with the n → π^* excited states of tetragonally symmetric MEL_4X and ME_2L_4 complexes has been described in detail. (See: Miskowski, V. M.; Hopkins, M. D.; Winkler, J. R.; Gray, H. B. In *Inorganic Electronic Structure and Spectroscopy*, Vol. II.; Solomon, E. I., Lever, A. B. P., Eds.; Wiley: New York, 1999; pp 343−402.)